

Nanobowl optical concentrator for efficient light trapping and high-performance organic photovoltaics

[Yongcai Qiu](#), [Siu-Fung Leung](#), [Qianpeng Zhang](#), [Cheng Mu](#), [Bo Hua](#), [He Yan](#), [Shihe Yang](#) and [Zhiyong Fan](#)

Citation: [Science Bulletin](#) **60**, 109 (2015); doi: 10.1007/s11434-014-0693-8

View online: <http://engine.scichina.com/doi/10.1007/s11434-014-0693-8>

View Table of Contents: <http://engine.scichina.com/publisher/scp/journal/SB/60/1>

Published by the [Science China Press](#)

Articles you may be interested in

[Design and fabrication of 1-D semiconductor nanomaterials for high-performance photovoltaics](#)

[Science Bulletin](#) **61**, 357 (2016);

[Development of small-molecule materials for high-performance organic solar cells](#)

[SCIENCE CHINA Chemistry](#) **58**, 922 (2015);

[Non-fullerene small molecule electron acceptors for high-performance organic solar cells](#)

[Journal of Energy Chemistry](#) **27**, 990 (2018);

[Optimal bulk-heterojunction morphology enabled by fibril network strategy for high-performance organic solar cells](#)

[SCIENCE CHINA Chemistry](#)

[Ag nanoparticles preparation and their light trapping performance](#)

[SCIENCE CHINA Technological Sciences](#) **56**, 109 (2013);



NENS 2019

The 4th International Conference on
Nanoenergy and Nanosystems(NENS)

June 15-17, 2019 Beijing, China

Nanobowl optical concentrator for efficient light trapping and high-performance organic photovoltaics

Yongcai Qiu · Siu-Fung Leung · Qianpeng Zhang ·
Cheng Mu · Bo Hua · He Yan · Shihe Yang ·
Zhiyong Fan

Received: 15 November 2014 / Accepted: 25 November 2014 / Published online: 31 December 2014
© Science China Press and Springer-Verlag Berlin Heidelberg 2014

Abstract Geometrical light trapping is a simple and promising strategy to largely improve the optical absorption and efficiency of solar cell. Nonetheless, implementation of geometrical light trapping in organic photovoltaic is challenging due to the fact that uniform organic active layer can rarely be achieved on textured substrate. In this work, squarely ordered nanobowl array (SONA) is reported for the first time and [6,6]-phenyl-C₆₁-butyric acid methyl ester (PCBM):poly(3-hexylthiophene) (P3HT)-based organic photovoltaic (OPV) device on SONA demonstrated over 28 % enhancement in power conversion efficiency over the planar counterpart. Interestingly, finite-difference time-domain (FDTD) optical simulation revealed that the superior light trapping by SONA originated from optical concentrator effect by nanobowl. Furthermore, aiming at low-cost, solution processible, and resource sustainable flexible solar cells, we employed Ag nanowires for the top transparent conducting electrode. This work not only revealed the in-depth understanding of light trapping by nanobowl optical concentrator, but also demonstrated the feasibility of implementing geometrical light trapping in OPV.

Keywords Nanobowl · Optical concentrator · Anodic aluminum oxide · Flexible photovoltaic · Organic solar cells

1 Introduction

Solar energy is one of the most promising renewable energy resources and represents a clean and ultimate replacement for fossil fuels in the future [1]. Over the past decades, enormous efforts have been invested in developing efficient and cost-effective photovoltaic (PV) devices which are competitive to the fossil fuel [2–6]. Organic photovoltaic (OPV) has been regarded as one of the promising candidates for large-scale, low-cost, and efficient solar energy harvesting [7–24]. Typical OPV devices are fabricated on conducting indium-doped SnO₂ (ITO)-coated glasses or transparent plastics [25]. However, indium is rare on earth, and the sheet resistance of ITO on plastics is relatively high, which compromises OPV device performance [26]. Comparatively, a metal foil substrate has the advantages of excellent conductivity, robust mechanical flexibility, cost-effectiveness, good thermal stability, and roll-to-roll processibility [27, 28]. In the past ten years, enormous efforts have been directed on inverted OPV devices and different metal substrates have been explored. Among those metals, aluminum is favorable due to its low cost, light weight and excellent flexibility. Meanwhile, light trapping by textured substrate is an appealing strategy to improve solar cell efficiency. In this regard, several unique nanophotonic structures have been developed on aluminum substrate using anodization [29–36]. After aluminum anodization and removal of alumina, three-dimensional nanostructures, such as nanospike and nanoconcave, can be obtained. The effectiveness of these nanostructures

Electronic supplementary material The online version of this article (doi:10.1007/s11434-014-0693-8) contains supplementary material, which is available to authorized users.

Y. Qiu · C. Mu · H. Yan · S. Yang (✉)
Department of Chemistry, The Hong Kong University of Science and Technology, Hong Kong, China
e-mail: chsyang@ust.hk

Y. Qiu · S.-F. Leung · Q. Zhang · B. Hua · Z. Fan (✉)
Department of Electronic and Computer Engineering,
The Hong Kong University of Science and Technology,
Hong Kong, China
e-mail: eezfan@ust.hk

for improving performance of inorganic thin-film solar cells had been demonstrated [29, 37]. However, application of these nanostructures for OPV has yet been successfully demonstrated up to now. This is partly due to the more stringent requirement on active layer thickness uniformity for OPV devices, and such uniformity is hard to be guaranteed on high aspect ratio nanostructures with the existing coating techniques. Recently, we combined nanoimprint technique and newly developed aluminum anodization to fabricate squarely ordered nanobowl array (SONA) on low-cost, light-weight, and flexible aluminum foil. In particular, such nanobowl architecture could act as a nanoscale optical concentrator and trap the incident light. Toward the application for OPV, SONA could improve optical absorption in photoactive layer and allow deposition of uniform and high-quality active materials because of the relatively smooth structure as compared to nanospikes or nanocones. Herein, we reported the flexible OPV devices fabricated on SONA substrates, and PCBM:P3HT was used as the photoactive layer for the proof of principle in OPV. On the other hand, targeting on low-cost, solution processible, and resource sustainable flexible solar cells, we employed Ag nanowire for the top transparent conducting electrode. More importantly, through simulations and experiments, we demonstrated significantly improved optical absorption and power conversion efficiency (PCE) of OPV devices.

2 Experiments

The fabrication procedure of the SONA-based OPV cell is briefly described in Fig. 1a, and the detail process can be found in Sect. 3. Briefly, the process comprises: (i) Nanoimprint using silicon stamp to produce nanodot array on clean aluminum foil. Thereafter, aluminum foil with hole array on the surface was anodized in appropriate electrolyte

and voltage; (ii) Removal of anodic alumina membrane by wet chemical etching to expose the SONA; (iii) Sputtering Cr or Pt thin films and ultrasonic spray pyrolysis (USP) deposition of a ZnO film; (iv) Spin-coating of polymer active layer (PCBM:P3HT and poly(3,4-ethylenedioxythiophene)/poly(styrenesulfonate) (PEDOT:PSS)) on a SONA substrate; and (v) Deposition of Ag nanowires (NW) as top electrode. The corresponding band diagrams of the desired OPV cells are shown in Fig. 1b. The generated holes can migrate to Ag nanowire electrode through the PEDOT:PSS layer, while the photoexcited electrons could transport through ZnO layer to the Pt-coated Al substrate (Fig. 1b). The key of fabricating SONA relies on the regular hole array created by nanoimprint on aluminum surface using silicon stamp prior to the aluminum anodization, and Fig. 2a shows the top view SEM image of aluminum surface after nanoimprint. It is worth pointing out that the pitch of SONA was controlled by the pitch of nanodot array on the nanoimprint stamp. In order to study the relationship between the pitch of SONA and OPV device performance, SONA with pitch of 1,000, 1,200, and 1,500 nm is fabricated and showed in Fig. 2b–d, respectively. Furthermore, atomic force microscopy (AFM) was performed to study the morphologies of SONA. Figure S1 (Online) presents the AFM image and Z-height analysis of SONA with 1,000-nm pitch. As shown in the AFM data, 1,000-nm-pitch SONA had a fixed nanobowl height of 225 nm and therefore it is named as P1000-H225 in the following text. The heights of nanobowl for rest of the pitches are plotted in Fig. S2 (Online), and 1,200- and 1,500-nm-pitch SONA have been named as P1200-H260 and P1500-H325, respectively. As shown in Fig. S2 (Online), the nanobowl height monotonically depends on the pitch of SONA. For the OPV device fabrication, since there is usually a thin layer of native oxide on the Al surface, a 20-nm-thick Pt layer was deposited on the SONA by sputtering followed by ZnO coating. This ZnO layer of

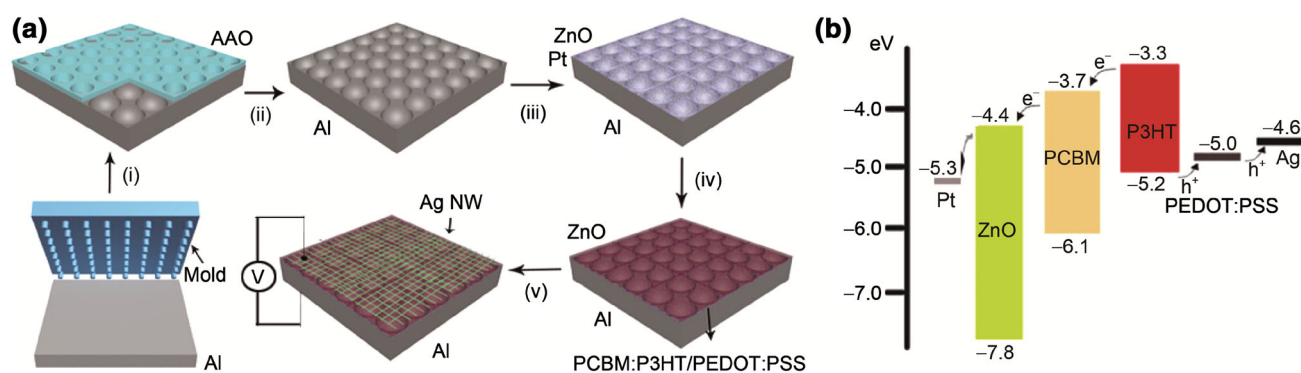


Fig. 1 SONA-based OPV cell. **a** Schematic diagram showing the fabrication process of SONA-based OPV cell. (i) Nanoimprint and anodization. (ii) Removal of anodic alumina membrane to expose the underneath nanobowl. (iii) Deposition of ZnO hole-blocking layer by ultrasonic spray pyrolysis (USP). (iv) Spin-coating of polymer active layer (PCBM:P3HT and PEDOT:PSS) and (v) Ag NW deposition. **b** The corresponding band diagrams of the desired OPV device

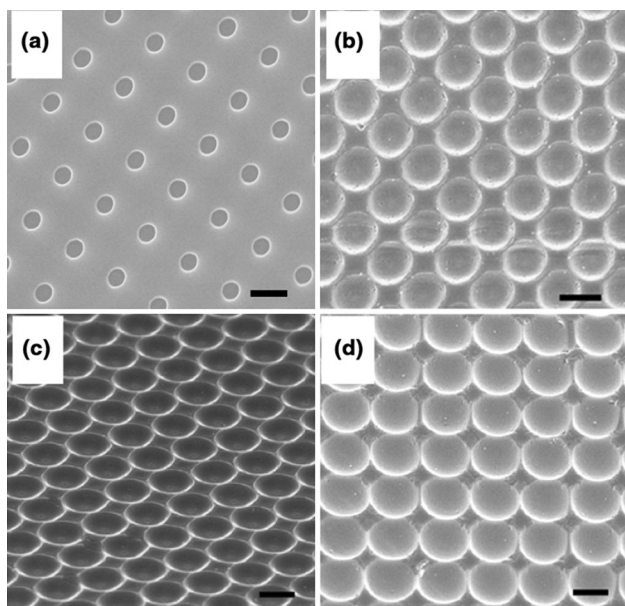


Fig. 2 SEM images of the SONA with different pitches. **a** SEM top view of aluminum surface after nanoimprint. **b** SEM top view of SONA with pitch of 1,000 nm and height of ~ 225 nm. **c** Tilting SEM view of SONA with pitch of 1,200 nm and height of ~ 260 nm. **d** SEM top view image of SONA with a pitch of 1,500 nm and a height of ~ 325 nm. All scale bars shown here were 1 μm

about 30 nm thick serves as a hole-blocking layer and was coated by the USP technique as mentioned above. And the uniformity of the ZnO layer is clearly evidenced in Fig. S3 (Online), which essentially replicated the original morphology of the SONA. Therefore, it was concluded that the simple USP technique can provide metal-oxide coating with extraordinary uniformity, and in our previous reports, we have demonstrated that USP technique worked perfectly with high aspect ratio nanostructure as well [38, 39].

In order to explore OPV application of SONA substrates, OPV devices were fabricated on the SONA substrates using standard photoactive materials: P3HT as electron donor and PCBM as electron acceptor. Specifically, PCBM:P3HT was spin-coated on SONA substrates, followed by PEDOT:PSS, and then, Ag NW were prepared using polyvinyl pyrrolidone (PVP) as structure-directing reagent [40–43]. The device configuration could be represented as SONA substrate/Pt/ZnO/photoactive layer/PEDOT:PSS/Ag NW, as shown in Fig. 1a.

3 Materials and methods

3.1 Preparation of SONA

Aluminum (Al) foil was cut into 2 cm by 2 cm pieces and cleaned in acetone and isopropyl alcohol. The sheets were

electrochemically polished in a 1:3 (v:v) mixture of perchloric acid and ethanol for 2 min at 10 °C. The polished Al foils were imprinted by silicon molds (squarely ordered pillar array with height of 200 nm, pitches of 1,000, 1,200 and 1,500 nm and a pressure of about 2×10^4 N cm^{-2} to initiate the perfectly ordered anodic alumina membrane (AAM) growth). Then, the Al sheets were anodized with homebuilt anodization setup. For the growth of SONA with a pitch of 1,000 nm, anodization was carried out at a 200-V voltage and in a mixture of 1.5 mL of 1 % H_3PO_4 , 1:1 v/v % of 1 % citric acid and ethylene glycol (total volume: 240 mL) at 10 °C for 20 min; for the growth of SONA with a pitch of 1,200 nm, anodization was carried out at a 240–360 V voltage and in a mixture of 1 mL of 1 % H_3PO_4 , 1:1 v/v % of 1 % citric acid and ethylene glycol (total volume: 240 mL) at 10 °C for 20 min. For the growth of SONA with a pitch of 1,500 nm, anodization was carried out at a 300-V voltage and in a mixture of 0.5 mL of 1 % H_3PO_4 , 1:1 v/v % of 1 % citric acid and ethylene glycol (total volume: 240 mL) at 10 °C for 20 min. Carbon rod was used as the counter electrode. For the exposure of SONA, the AAM film was etched in a mixture of chromic acid (1.5 wt%) and phosphoric acid (6 wt%) solutions at 100 °C for 20 min. After etching, the SONA were cleaned with DI water and blown dry with air for the subsequent thin-film deposition.

3.2 Preparation of Ag nanowires as transparent conducting electrode

The Ag nanowires were prepared using polyvinyl pyrrolidone (PVP) as structure-directing reagent. To obtain long/thin Ag NW for OPV cells, controlled centrifugal separation was carried out at a low speed of 4,000 r min^{-1} . The as-obtained long/thin Ag NW could achieve a high transmission of over 90 % at 550 nm wavelength and a low sheet resistance of 13.8 $\Omega \text{ cm}^{-2}$ (Fig. S4 online).

3.3 Preparation of SONA-based OPV cells

A 20-nm-thick Pt layer was first coated on SONA by magnetron sputtering. Second, an approximately 30-nm-thick ZnO layer was deposited on SONA by ultrasonic spray pyrolysis (USP) using a methanol solution of zinc acetate (5 mmol L^{-1}). Third, a 1,2-dichlorobenzene solution (1 mL) of P3HT (10 mg) and PCBM (20 mg) was spin-coated on the SONA with ZnO layer in a glove box and annealed at 150 °C for 10 min to form a uniform polymer bulk heterojunction layer on top of ZnO. Afterward, the samples were moved out of the glove box, followed by an about 50-nm-thick PEDOT:PSS buffer

layer spin-coating on top of the active layer and was annealed at 120 °C for 5 min afterward. Finally, Ag NW dispersed in isopropyl alcohol (IPA) (1 mg mL⁻¹) was spin-coated on top of the buffer layer and was then annealed at 120 °C for 5 min in a glove box. The active area was defined by the shadow mask with areas of (3 × 3) mm².

3.4 Characterization

Morphologies of the nanomaterials were directly examined by SEM using a JEOL6700F at an accelerating voltage of 5 kV. Diffused reflectance spectra were carried out on the same film samples using a Perkin–Elmer UV–vis spectrophotometer (model Lambda 20). Solar simulator (Oriol solar simulator, 450 W Xe lamp, AM 1.5 global filter) was calibrated to 1 sun (100 mW cm⁻²) using an optical power meter (Newport, model 1916-C) equipped with a Newport 818P thermopile detector. Two electrode terminals were made by connecting one end of Ag NW net and the other end of thin Pt layer on Al substrate both by Ag paste. The electrochemical spectra were measured by the Zahner Zennium C-IMPS system.

4 Results and discussion

Figure 3a, b shows the SEM top view and optical image of the SONA-based OPV device. To examine the optical absorption enhancement of SONA-based OPV device, UV–vis absorbance was measured and the absorption spectra are presented in Fig. 3c. Apparently, optical absorptions of the SONA-based OPV devices were much better than that of the flat counterpart especially at long wavelength beyond 620 nm. Among three kinds of pitches of SONA, P1000-H225 showed slightly higher optical absorption than the rest of the two pitches which is consistent with the optical studies of our previous report [30]. To further shed light on the absorption enhancement, three-dimensional finite-difference time-domain (FDTD) simulations were performed on a variety pitch of SONA devices [44]. In particular, carrier generation rates (GR) profiles were calculated by assuming that each photon absorbed within the semiconductor creates one electron–hole pair, and the field profiles at 400–700 nm were used to calculate the GR per unit volume:

$$\text{GR} = \int_{\text{Solar spectrum}} \left(\frac{\epsilon'' |\vec{E}(\omega)|^2}{2\hbar} \right),$$

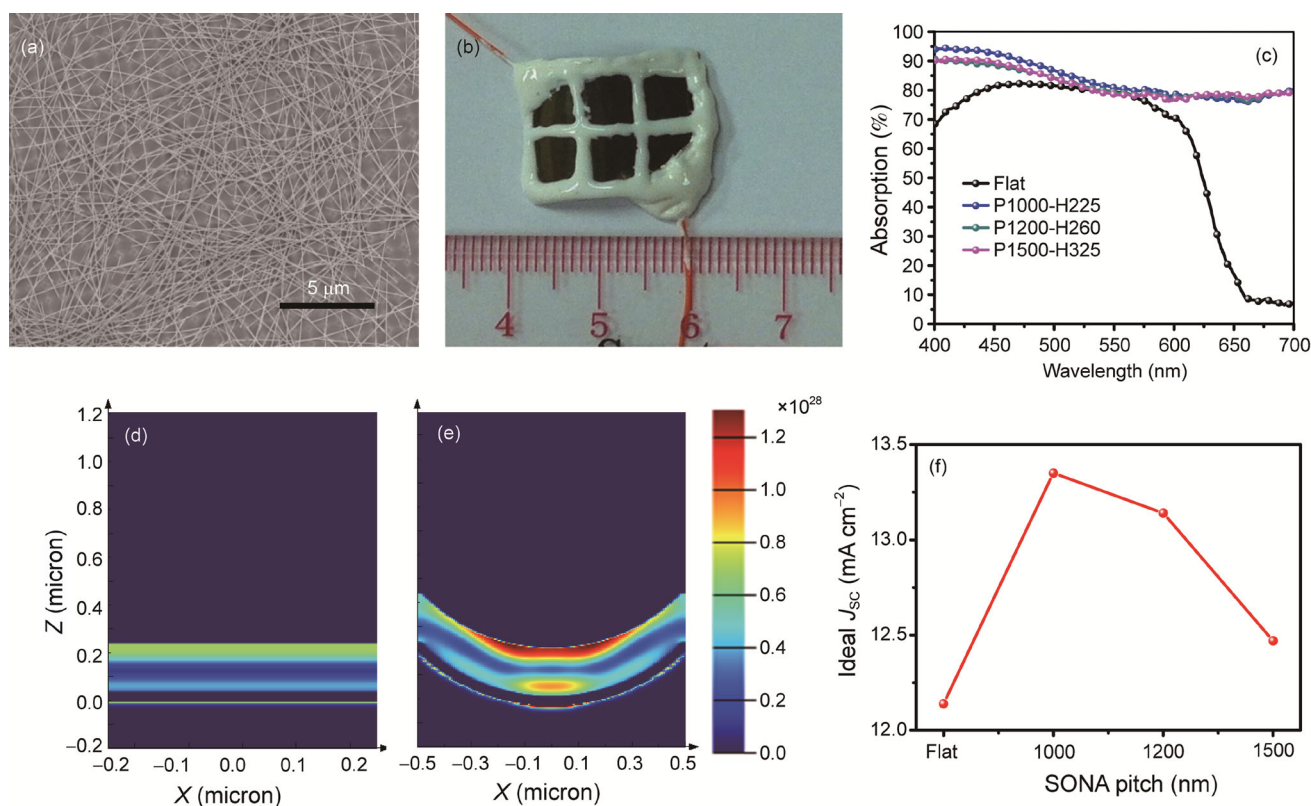


Fig. 3 Optical characterization and simulations. **a, b** SEM top view and optical image of SONA-based OPV cell, respectively. **c** Optical absorption spectra of flat and SONA-based OPV devices with different pitches. **d, e** Cross-sectional generation rates profile of flat and P1000-H225 OPV device. **f** Calculated ideal J_{sc} of flat and SONA-based OPV devices from GR simulation

where $|\vec{E}(\omega)|^2$ is the magnitude of the electric field squared within the structure resulting from solar illumination and ε'' is the imaginary part of the dielectric function of the semiconductor.

Displayed in Fig. 3d–e are the cross-sectional GR profiles of OPV devices on flat and P1000-H225, respectively. Notably, it can be observed from the color index that the GR in P1000-H225 is significantly higher than the flat counterpart. The superior GR of P1000-H225 over flat can be attributed to the focusing of incident light within the photoactive layer by the concave mirror-like nanobowl concentrator. The focusing effect by the nanobowl can be further evidenced by the concentrated generation at the central region of the photoactive layer which corresponds to the focal point of concave mirror. Cross-sectional GR profile of devices on P1200-H260 and P1500-H325 are shown in Fig. S5 (Online), and they also showed higher GR over flat control. In order to identify SONA substrate with the best light trapping capability, the ideal short-circuit current density (J_{sc}) of each candidates was calculated by assuming that generated electron–hole pair was entirely contributed to the current and the results are shown in Fig. 3f. Intriguingly, P1000-H225 has the highest ideal J_{sc} among all SONA substrates and the ideal J_{sc} decreased with increasing the SONA pitch. This result can be explained by the up-shifted focusing point out of photoactive layer due to increased diameters of nanobowl concentrator for P1200-H265 and P1500-H325. Furthermore, SONA structures also provided efficient light trapping at various incident angles which are of crucial importance from practical perspective as sunlight incident angle varies throughout the day [34, 45]. As revealed from angular-dependent reflectance measurement in Fig. S6 (online), reflectance of SONA-based OPV device remained low even at oblique incident angle. Moreover, the promising light trapping capability of SONA substrate was further proven by their PV performance. OPV devices fabricated on SONAs were characterized under AM 1.5G illumination (100 mW cm^{-2}). Figure 4a presents the current density–voltage (J – V) characteristic of SONA-based and flat control OPV devices, and their corresponding electrical parameters are summarized in Table 1. The flat OPV cell showed a J_{sc} of about 8.31 mA cm^{-2} , open-circuit voltage (V_{oc}) of about 0.57 V, and fill factor (FF) of about 51.2 %, achieving an overall power conversion efficiency (PCE) of about 2.43 %. With improved light trapping by nanobowl concentrator, P1000-H225-based OPV cells had much stronger photon absorption in photoactive layer leading to the highest J_{sc} of $\sim 9.41 \text{ mA cm}^{-2}$ among all SONA substrates, which showed 13.2 % enhancement as compared to the flat control. With $V_{oc} \sim 0.573 \text{ V}$ and FF $\sim 57.9 \%$, this champion device yielded a PCE $\sim 3.12 \%$.

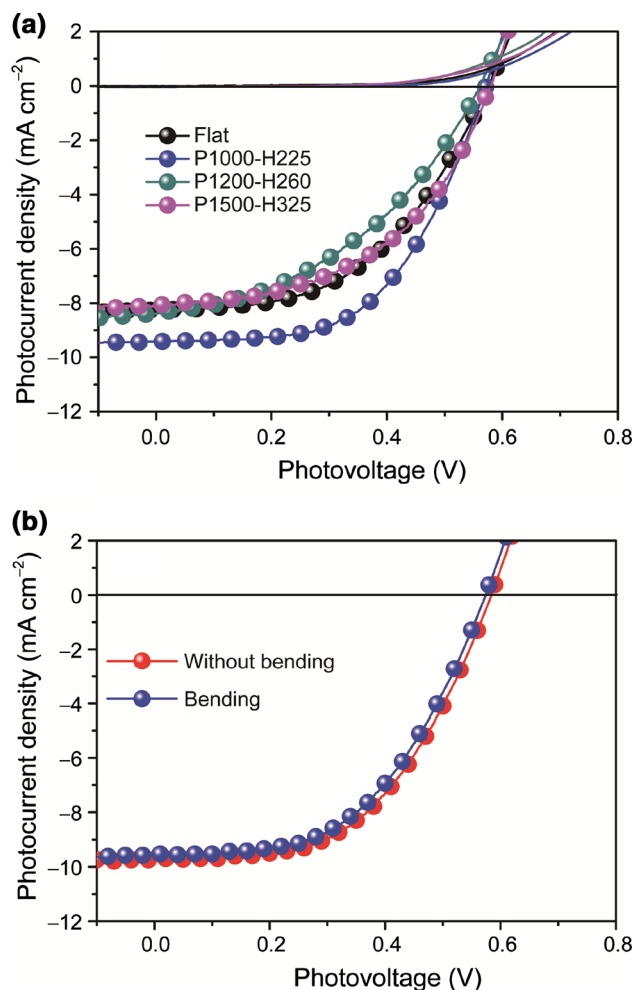


Fig. 4 Photovoltaic performance characterization. **a** J – V curves of the best-performance device in different pitches SONA. **b** J – V curves of a flexible SONA OPV device with and without bending

Table 1 Photovoltaic characteristics of the OPV devices under AM 1.5G illumination (100 mW cm^{-2})

Device	J_{sc} (mA cm^{-2})	V_{oc} (V)	FF (%)	PCE (%)
Flat	8.31	0.571	51.2	2.43
P1000-H225	9.41	0.573	57.9	3.12
P1200-H260	8.45	0.560	43.8	2.07
P1500-H325	8.01	0.578	50.8	2.35

The values are the averages of three most efficient samples of each candidate

The enhanced performance by P1000-H225 SONA is further evidenced by incident photon-to-electron conversion efficiency (IPCE) measurement shown in Fig. S7 (Online). In contrast, J_{sc} of OPV devices fabricated on P1200-H260 and P1500-H315 was lower than that on P1000-H225 which agreed with the GR simulation. It is worth noting that the FF of OPV devices fabricated on P1200-H260 and

P1500-H315 were lower than that on P1000-H225 which can be attributed to the thicker spin-coated photoactive layer at their relatively deeper nanobowl for large-pitch SONAs and therefore resulting in significantly lower fill factor. As revealed in the UV–vis measurement, SONA-based OPV devices exhibited prominent light scattering in red light region above 620 nm. Previously, aluminum has served as a flexible substrate in CdS pillar array–CdTe PVs and a-Si PV [46, 47]. Similarly, the SONA-based OPV cell has excellent flexibility which can be demonstrated by the J – V characteristics shown in Fig. 4b. Notably, the bending only affected the device performance marginally, thus suggesting that the SONA could serve as a flexible substrate for low-cost OPV cells.

5 Conclusions

We have demonstrated the potency and capabilities of flexible polymer solar cell module fabricated on nanobowl substrates with PCBM:P3HT as a photoactive layer and Ag nanowires as a top transparent conducting electrode. The nanobowl structure exhibited intriguing light concentration effect thus leading to over 28 % improvement of performance of the OPV devices. To our best knowledge, this effect has rarely been reported and harnessed previously for photovoltaics. The simplicity of structure fabrication and its attractive effectiveness on light trapping offers a promising path for large-scale production of high-performance flexible PV cells.

Acknowledgments This work was supported by the HK-RGC General Research Funds (HKUST 605710, 604809, 612111, 612113), and partially supported by ITS/117/13 from Hong Kong Innovation Technology Commission.

Conflict of interest The authors declare that they have no conflict of interest.

References

- Lewis NS, Nocera DG (2006) Powering the planet: chemical challenges in solar energy utilization. *Proc Natl Acad Sci USA* 103:15729–15735
- Kamat PV, Tvrđy K, Baker DR et al (2010) Beyond photovoltaics: semiconductor nanoarchitectures for liquid-junction solar cells. *Chem Rev* 110:6664–6688
- Shah A, Torres P, Tscharnner R et al (1999) Photovoltaic technology: the case for thin-film solar cells. *Science* 285:692–698
- Yeh LK, Lai KY, Lin GJ et al (2011) Giant efficiency enhancement of GaAs solar cells with graded antireflection layers based on syringelike ZnO nanorod arrays. *Adv Energy Mater* 1:506–510
- Wei W, Tsai M, Ho S et al (2013) Above-11 %-efficiency organic–inorganic hybrid solar cells with omnidirectional harvesting characteristics by employing hierarchical photon trapping structures. *Nano Lett* 13:3658–3663
- Leung S, Zhang Q, Xiu F et al (2014) Light management with nanostructures for optoelectronic devices. *J Phys Chem Lett* 5:1479–1495
- Li G, Shrotriya V, Huang JS et al (2005) High-efficiency solution processable polymer photovoltaic cells by self-organization of polymer blends. *Nat Mater* 4:864–868
- Ameri T, Li N, Brabec CJ (2013) Highly efficient organic tandem solar cells: a follow up review. *Energy Environ Sci* 6:2390–2413
- Angmo D, Larsen-Olsen TT, Jorgensen M et al (2013) Roll-to-roll inkjet printing and photonic sintering of electrodes for ITO free polymer solar cell modules and facile product integration. *Adv Energy Mater* 3:172–175
- Verreet B, Rand BP, Cheyns D et al (2011) A 4 % efficient organic solar cell using a fluorinated fused spherulocyanine dimer as an electron acceptor. *Adv Energy Mater* 1:565–568
- You J, Li X, Xie F et al (2012) Surface plasmon and scattering-enhanced low-bandgap polymer solar cell by a metal grating back electrode. *Adv Energy Mater* 2:1203–1207
- Ameri T, Dennler G, Lungenschmied C et al (2009) Organic tandem solar cells: a review. *Energy Environ Sci* 2:347–363
- Chen H, Hou J, Zhang S et al (2009) Polymer solar cells with enhanced open-circuit voltage and efficiency. *Nat Photonics* 3:649–653
- Günes S, Neugebauer H, Sariciftci NS (2007) Conjugated polymer-based organic solar cells. *Chem Rev* 107:1324–1338
- Cheng Y, Yang S, Hsu C (2009) Synthesis of conjugated polymers for organic solar cell applications. *Chem Rev* 109:5868–5923
- Han M, Kim H, Seo H et al (2012) Photovoltaic efficiency enhancement by the generation of an embedded silica-like passivation layer along the P3HT/PCBM interface using an asymmetric block-copolymer additive. *Adv Mater* 24:6311–6317
- Shelton SW, Chen TL, Barclay DE et al (2012) Solution-processable triindoles as hole selective materials in organic solar cells. *ACS Appl Mater Interfaces* 4:2534–2540
- Kim BJ, Miyamoto Y, Ma B et al (2009) Photocrosslinkable polythiophenes for efficient, thermally stable, organic photovoltaics. *Adv Funct Mater* 19:2273–2281
- Lan J, Cherng S, Yang Y et al (2014) The effects of Ta₂O₅–ZnO films as cathodic buffer layers in inverted polymer solar cells. *J Mater Chem A* 2:9361–9370
- Lan J, Liang Z, Yang Y et al (2014) The effect of SrTiO₃: ZnO as cathodic buffer layer for inverted polymer solar cells. *Nano Energy* 4:140–149
- Yao Y, Hou J, Xu Z et al (2008) Effects of solvent mixtures on the nanoscale phase separation in polymer solar cells. *Adv Funct Mater* 18:1783–1789
- Shrotriya V, Wu EH, Li G et al (2006) Efficient light harvesting in multiple-device stacked structure for polymer solar cells. *Appl Phys Lett* 88:064104
- Tan Z, Li L, Li C et al (2014) Trapping light with a nanostructured CeO_x/Al Back electrode for high-performance polymer solar cells. *Adv Mater Interfaces* 1:1400197
- Tan Z, Li L, Wang F et al (2014) Solution-processed rhenium oxide: a versatile anode buffer layer for high performance polymer solar cells with enhanced light harvest. *Adv Energy Mater* 4:1–7
- Kumar V, Wang H (2013) Selection of metal substrates for completely solution-processed inverted organic photovoltaic devices. *Sol Energy Mat Sol Cells* 113:179–185
- Chauhan RN, Singh C, Anand R et al (2012) Effect of sheet resistance and morphology of ITO thin films on polymer solar cell characteristics. *Int J Photoenergy* 2012:879261
- Lee MH, Lim N, Ruebusch DJ et al (2011) Roll-to-roll anodization and etching of aluminum foils for high-throughput surface nano-texturing. *Nano Lett* 11:3425

28. Søndergaard RR, Hösel M, Krebs FC (2013) Roll-to-Roll fabrication of large area functional organic materials. *J Polym Sci Part B: Polym Phys* 51:16–34
29. Leung S, Gu L, Zhang Q et al (2014) Roll-to-roll fabrication of large scale and regular arrays of three-dimensional nanospikes for high efficiency and flexible photovoltaics. *Sci Rep* 4:4243
30. Leung SF, Yu M, Lin Q et al (2012) Efficient photon capturing with ordered three-dimensional nanowell arrays. *Nano Lett* 12:3682–3689
31. Lin Q, Hua B, Leung S et al (2013) Efficient light absorption with integrated nanopillar/nanowell arrays for three-dimensional thin-film photovoltaic applications. *ACS Nano* 7:2725–2732
32. Lin Q, Leung S, Tsui K et al (2013) Programmable nanoengineering templates for fabrication of three-dimensional nanophotonic structures. *Nanoscale Res Lett* 8:268
33. Yu R, Ching K, Lin Q et al (2011) Strong light absorption of self-organized 3-D nanospike arrays for photovoltaic applications. *ACS Nano* 5:9291–9298
34. Tsui KH, Lin Q, Chou H et al (2014) Low-cost, flexible and self-cleaning three-dimensional anti-reflection nanocone arrays for high efficiency photovoltaics. *Adv Mater* 26:2805–2811
35. Lin Q, Leung S, Lu L et al (2014) Inverted nanocone-based thin film photovoltaics with omnidirectionally enhanced performance. *ACS Nano* 8:6484–6490
36. Guo R, Huang H, Chang P et al (2014) Coupled optical and electrical modeling of thin-film amorphous silicon solar cells based on nanodent plasmonic substrates. *Energy Environ Sci* 8:141–149
37. Huang H, Lu L, Wang J et al (2013) Performance enhancement of thin-film amorphous silicon solar cells with low cost nanodent plasmonic substrates. *Energy Environ Sci* 6:2965–2971
38. Qiu Y, Leung S, Zhang Q et al (2014) Efficient photoelectrochemical water splitting with ultra-thin film of hematite on three-dimensional nanophotonic structures. *Nano Lett* 14:2123–2139
39. Li J, Qiu Y, Wei Z et al (2014) Three-dimensional hexagonal fluorine-doped tin oxide nanocone arrays: a superior light harvesting electrode for high performance photoelectrochemical water splitting. *Energy Environ Sci* 7:3651–3658
40. Wei H, Huang J, Hsu C et al (2013) Organic solar cells featuring nanobowl structures. *Energy Environ Sci* 6:1192–1198
41. Hu L, Kim HS, Lee J et al (2010) Scalable coating and properties of transparent, flexible, silver nanowire electrodes. *ACS Nano* 4:2955–2963
42. Chen Y, Li Z, Chen X et al (2012) Improved performance of flexible amorphous silicon solar cells with silver nanowires. *J Appl Phys* 112:124320
43. Sun Y, Xia Y (2002) Large-scale synthesis of uniform silver nanowires through a soft, self-seeding, polyol process. *Adv Mater* 14:833–837
44. Dewan R, Marinkovic M, Noriega R et al (2009) Light trapping in thin-film silicon solar cells with submicron surface texture. *Opt Express* 17:23058–23065
45. Lin G, Wang H, Lien D et al (2014) A broadband and omnidirectional light-harvesting scheme employing nanospheres on Si solar cells. *Nano Energy* 6:36–43
46. Fan ZY, Razavi H, Do JW et al (2009) Three-dimensional nanopillar-array photovoltaics on low-cost and flexible substrate. *Nat Mater* 8:648–653
47. Leung S, Tsui K, Lin Q et al (2014) Large scale, flexible and three-dimensional quasi-ordered aluminum nanospikes for thin film photovoltaics with omnidirectional light trapping and optimized electrical design. *Energy Environ Sci* 7:3611–3616